

An adaptive spectral method for oscillatory second-order linear ODEs with frequency-independent cost

Fruzsina J. Agocs^{1,*} and Alex H. Barnett^{1,**}

¹Center for Computational Mathematics, Flatiron Institute, 162 Fifth Avenue, New York, 10010 NY, USA

*fagocs@flatironinstitute.org

**abarnett@flatironinstitute.org

Abstract

We introduce an efficient numerical method for second order linear ODEs whose solution may vary between highly oscillatory and slowly changing over the solution interval. In oscillatory regions the solution is generated via a nonoscillatory phase function that obeys the nonlinear Riccati equation. We propose a defect-correction iteration that gives an asymptotic series for such a phase function; this is numerically approximated on a Chebyshev grid with a small number of nodes. For analytic coefficients we prove that each iteration, up to a certain maximum number, reduces the residual by a factor of order of the local frequency. The algorithm adapts both the step size and the choice of method, switching to a conventional spectral collocation method away from oscillatory regions. In numerical experiments we find that our proposal outperforms other state-of-the-art oscillatory solvers, most significantly at low-to-intermediate frequencies and at low tolerances, where it may use up to 10^6 times fewer function evaluations. Even in high frequency regimes, our implementation is on average 10 times faster than other specialized solvers.

1 Introduction

The efficient numerical solution of highly oscillatory ordinary differential equations (ODEs) has long been a challenge. A wide range of specialized methods exists for dealing with ODEs with various structures; see [48, 22] for thorough reviews. In this work we handle a commonly occurring form, the variable-coefficient, linear, second order ODE with smooth coefficients. This includes simple harmonic oscillators with time-dependent coefficients, which arise in many computational physics problems. One application in which an extremely fast numerical solution is needed is Bayesian parameter estimation in cosmology. Specifically, each spatial Fourier mode of the density perturbations obeys such an ODE in time, with solutions that may switch repeatedly between smooth and highly oscillatory characters [3]. Of order 10^3 modes are needed, and this must be repeated for up to 10^6 trial parameter choices; thus the ODE solver may be called a billion times, and an efficient frequency-independent solver is crucial. Besides inflationary cosmology [37, 46, 55], this class of ODE appears in Hamiltonian dynamics [49, 24], particle accelerators and plasma physics [15, 16, 34, 42], electric circuits [43], satellite systems [50], acoustics and gravity waves [23, 21], and quantum mechanics [30, 1, 5, 14]. In many of these fields our proposed method could supply a robust and efficient numerical replacement for uncontrolled asymptotic approximations.

The ODE under study has the form

$$u''(t) + 2\gamma(t)u'(t) + \omega^2(t)u(t) = 0, \quad t \in (t_0, t_1) \subset \mathbb{R}, \quad (1)$$

where γ is a given smooth (by which we mean C^∞) damping function, and ω is a given smooth, but possibly very large, real-valued local frequency function¹. We solve the initial value problem (IVP)

$$u(t_0) = u_0, \quad (2)$$

$$u'(t_0) = u'_0, \quad (3)$$

although we note that the methods that we present could easily be applied to two-point boundary value problems. The restriction to real ω is not crucial, but avoids complications with exponentially large dynamic ranges (e.g., deeply evanescent regions) that we leave for future study.

In regions where $\omega \gg 1$, the solution u is oscillatory: loosely speaking, it has local approximate form $ae^{i\omega_0 t} + be^{-i\omega_0 t}$, where ω_0 is a local value of $\omega(t)$. Conventional ODE integrators then require discretization with several grid points per local period $2\pi/\omega_0$, forcing the overall cost to be $\mathcal{O}(\omega_0)$, which can be prohibitively slow. This has led to the development of solvers that exploit new representations or asymptotic expansions of the solution, allowing many periods between discretization nodes. We now review such prior work, while noting that, to our knowledge, our proposal is the first to tackle the problem adaptively with spectral accuracy when the solution has both highly oscillatory and smooth regimes.

The most common asymptotic expansion is the Wentzel–Kramers–Brillouin (WKB), a perturbation method applied to linear differential equations that contain a small parameter in the highest derivative [7, 44]. This approximation arose in quantum mechanics where it is still widely applied for approximate analytic solutions of the Schrödinger equation. Writing $\omega(t) = \omega_0 \Omega(t)$, where $\Omega(t)$ is of unit size, and the asymptotic parameter is $\omega_0 \gg 1$, (1) becomes

$$u'' + 2\gamma(t)u' + \omega_0^2 \Omega(t)^2 u = 0. \quad (4)$$

Substituting $u(t) = e^{\omega_0 z(t)}$ and defining $z'(t) = x(t)$ gives the Riccati equation (a nonlinear 1st-order ODE) for x ,

$$x' + 2\gamma(t)x + \omega_0 x^2 + \omega_0 \Omega(t)^2 = 0. \quad (5)$$

Making a regular perturbation expansion in $1/\omega_0$,

$$x(t) = \sum_{j=0}^N \omega_0^{-j} x_j(t), \quad (6)$$

and matching powers of ω_0 in (4) gives the recursion relation for the functions $x_j(t)$ (where for simplicity we give only the $\gamma \equiv 0$ case),

$$x_0 = \pm i\Omega, \quad x_j = -\frac{1}{2x_0} \left(x'_{j-1} + \sum_{k=1}^{j-1} x_k x_{j-k} \right), \quad \text{for } j = 1, 2, \dots \quad (7)$$

Although originally an analytic tool, WKB has recently been exploited in numerical solvers. These algorithms achieve $\mathcal{O}(1)$ (*i.e.* ω_0 -independent) runtime in regions where the asymptotic series is a sufficiently good approximation. WKB forms the basis of the method described in [2, 3], and associated open-source software package `oscodel` [4]. This uses the expansion (6) up to and including x_3 within a time-step, or, if this is not accurate enough, switches to a 4,5th order Runge–Kutta pair. In [5, 38] the related “WKB marching method” uses the same expansion truncated after x_2 to transform (4) into a smoother problem in the highly oscillatory regions, otherwise again switching to a 4,5th order Runge–Kutta method. In terms of the stepsize h , neither method is formally high-order. `oscodel` has $\mathcal{O}(h)$ global error, although its prefactor is small when ω_0 is large. The

¹If coefficients are merely piecewise smooth, a solution may simply be patched together at the breakpoints, thus we do not discuss this situation further.

WKB-marching method’s oscillatory solver improves on this and has $\mathcal{O}(h^2)$ global error, resulting in better performance at lower tolerances.

Yet, as a consequence of low h order and fixed asymptotic order, a small requested tolerance in either method forces $h \lesssim 1/\omega_0$, removing the efficiency advantage over conventional timesteppers. They are therefore only efficient if no more than about 6 digits of accuracy are required, and can suffer at low-to-intermediate frequencies where more asymptotic terms would be required. The present method, on the other hand, is both spectrally accurate and adaptive in the number of terms in its asymptotic expansion.

The “quasilinearization method” (QLM) [6] instead successively approximates a solution of the Riccati equation (5) by a functional Newton iteration. The resulting differential equation recurrence (here stated for $\gamma \equiv 0$),

$$x_0 = \pm i\omega, \quad x'_j - x_{j-1}^2 + 2x_j x_{j-1} + \omega^2 = 0, \quad \text{for } j = 1, 2, \dots \quad (8)$$

turns out to yield a solution equivalent to a WKB expansion with 2^j terms. This recurrence is either solved symbolically [45, 41] or numerically [40, 39]. The former requires increasing amounts of algebra with iteration number, so can become cumbersome. Integrating each ODE in (8) numerically does not prove to be a better strategy since each such ODE is itself oscillatory.

Recently Bremer [11], following [35, 13], has proposed an efficient method for solving (1), in the special case $\gamma \equiv 0$, over a domain in which the solution is highly oscillatory. The method aims to find a global nonoscillatory phase function $\alpha(t)$ satisfying Kummer’s equation,

$$\frac{3}{4} \left(\frac{\alpha''}{\alpha'} \right)^2 - \frac{1}{2} \frac{\alpha'''}{\alpha'} - (\alpha')^2 + \omega(t)^2 = 0, \quad (9)$$

a nonlinear and generally oscillatory ODE, and will therefore be referred to as the Kummer’s phase function method hereafter. One then reconstructs solutions via $u(t) = \sin(\alpha(t) + c)/\sqrt{\alpha'(t)}$. The generated phase functions are nonoscillatory in the sense that they can be accurately approximated on intervals of fixed size using polynomials of degree independent of ω_0 . The results of [35, 13] prove the existence of such nonoscillatory phase functions when $\Omega(t)$ is nonoscillatory in the sense that $\log \Omega$ is smooth and its Fourier transform rapidly decaying. Finding initial conditions on the phase function leading to a nonoscillatory solution is, however, challenging. Bremer proposed a “windowing” method to numerically find such a global phase function on the interval (t_0, t_1) , first using a C^∞ partition of unity near t_1 to smoothly “blend” Ω to a constant function, integrating backwards from this constant region down to $t = t_0$, and finally integrating $t \in (t_0, t_1)$ forward using the original Ω . This exploits two facts: a nonoscillatory phase function for the constant case $\Omega(t) \equiv 1$ is simple to write down, and a smooth window allows the nonlinear Kummer oscillator to make a smooth (“adiabatic”) transition which excites only an exponentially small oscillation amplitude. The parameters of this partition of unity require problem-dependent adjustment. Nevertheless Bremer’s is the most efficient and accurate prior method known to the authors².

Here we present an approach using an asymptotic expansion for the derivative of a nonoscillatory Riccati phase function, meaning that we construct an expansion for $x(t) = (\log u(t))'$, the phase function being $z(t) = \log u(t) = \int^t x(\sigma) d\sigma$. An asymptotic sequence of functions approximating $x(t)$ is constructed via a defect correction scheme [9], where each iteration involves simply taking a derivative (performed numerically on a spectral grid), rather than solving an ODE as in QLM. We adaptively terminate this (non-convergent) iteration before it becomes unstable. Our algorithm is capable of handling a non-zero damping term γ , allowing for the direct solution of a wider range of second order linear ODEs than the WKB-marching or the Kummer’s phase function method. Our iteration does not introduce oscillatory contributions, hence finds a nonoscillatory approximate

²During the preparation of this manuscript, a new and more general phase function-based method able to tackle zeros in ω has been proposed by Bremer [12]. No comparison to this novel solver is made in this work due to its current lack of a publicly available implementation.

phase function without reference to initial conditions, in contrast to the Kummer’s phase function method. Another crucial difference from the latter is that $x(t)$ is solved for locally on one interval with an adaptively-chosen length, rather than globally. Solutions to (1)–(3) are then constructed by time-stepping over the integration range, repeatedly matching Cauchy data at interval endpoints. Our iteration only involves one previous term (a 2-term recurrence), so is simpler than the traditional WKB expansion (7) requiring all past terms.

Phase function methods, as with WKB or QLM methods, is naturally only applicable in the high frequency regime. Thus, a significant part of this work is to generalize ideas from [2] to create a fully adaptive algorithm that can switch between oscillatory and nonoscillatory methods, and choose the time-step h to achieve a user-requested tolerance efficiently. Our nonoscillatory method is a standard adaptive spectral collocation scheme.

This paper is structured as follows. Section 2 describes the various numerical methods used in the proposed algorithm including the asymptotic expansion for oscillatory domains, the spectral method based on Chebyshev nodes, adaptive control of stepsize, and switching between the two alternative schemes. Section 3 presents rigorous bounds (given analytic coefficients) on the Riccati residual under our defect correction scheme, including a bound $\mathcal{O}(e^{-c\omega_0})$ given sufficient terms. We show results from numerical experiments in Section 4, which involves a comparison with state-of-the-art ODE solvers mentioned above. Section 5 concludes with a summary and suggestions for future work.

2 Methods

2.1 Defect correction of the Riccati phase function

In this section we explain how to solve for a nonoscillatory Riccati phase function on an interval, which will correspond to a single time-step of the overall ODE solver. This interval has to be sufficiently small so that changes in the coefficients $\omega(t)$, $\gamma(t)$ are small, yet it has to contain a large number of oscillations of $u(t)$, so that $\omega(t)$ is sufficiently large. Writing $u = e^z$ where $x(t) = z'(t)$ is the derivative of the phase function $z(t)$, any nonvanishing $u(t)$ satisfies (1) if and only if $x(t)$ satisfies the nonlinear Riccati equation

$$x' + x^2 + 2\gamma(t)x + \omega(t)^2 = 0. \tag{10}$$

(For convenience we now work without rescaling by ω_0 as in Section 1.) A generic solution to (10) is oscillatory on the local timescale $1/\omega(t)$. This is illustrated by the case of constant $\omega \equiv \omega_0$ and $\gamma \equiv 0$, which has only the family of analytic solutions $x(t) = \omega_0 \tan(\alpha - \omega_0 t)$ parameterized by $\alpha \in \mathbb{C}$, where $\text{Re } \alpha$ is interpreted as a phase shift and $\text{Im } \alpha$ controls the amplitude. Their oscillation frequency is $2\omega_0$. However, taking the limit $\text{Im } \alpha \rightarrow \pm\infty$ produces the only two nonoscillatory (constant) solutions $x(t) = \pm i\omega_0$. For general analytic frequency functions $\omega(t)$ there also exist nonoscillatory solutions. These take the approximate form $x_{\pm}(t) \approx \pm i\omega(t)$, leading to a conjugate pair of basis functions $u_{\pm}(t) := \exp(\int^t x_{\pm}(\sigma) d\sigma)$. The rigorous existence of nonoscillatory solutions follows from the corresponding result for Kummer’s equation (9) proven in [35, 13]. The argument that existence of a real-valued Kummer’s phase function implies existence of a Riccati phase function goes as follows:³ if $\alpha(t)$ satisfies (9), then defining $\beta' = -\alpha''/2\alpha'$ allows (9) to be written $\beta'' - (\alpha')^2 + (\beta')^2 + \omega(t)^2 = 0$, and these last two equations are the real and imaginary parts of (10) with $x = i\alpha' + \beta'$.

Given any trial solution x to (10), we define its *residual* as the left-hand-side of (10), namely

$$R[x](t) := x' + x^2 + 2\gamma(t)x + \omega(t)^2. \tag{11}$$

³We thank Jim Bremer for explaining this argument to us.

We propose the following iteration to generate a sequence of functions x_0, x_1, \dots, x_k on a given interval, using the above positive (say) approximate form as a starting point:

$$x_0(t) = +i\omega(t), \quad (12)$$

$$x_{j+1}(t) = x_j(t) - \frac{R[x_j](t)}{2(x_j(t) + \gamma(t))}, \quad j = 0, 1, \dots, k-1. \quad (13)$$

This is an *approximate* Newton iteration for (10) (note that an exact Newton iteration has been used numerically [40, 39] and as an analysis tool [35]). To show this, perturbing x_j by a function δ_j we get

$$\begin{aligned} R[x_j + \delta_j] &= x'_j + \delta'_j + x_j^2 + 2x_j\delta_j + \delta_j^2 + 2\gamma x_j + 2\gamma\delta_j + \omega(t)^2 \\ &= R[x_j] + \delta'_j + 2x_j\delta_j + 2\gamma\delta_j + \mathcal{O}(\delta_j^2), \end{aligned}$$

then linearization yields a linear first order ODE for δ_j , $\delta'_j + 2x_j(t)\delta_j + 2\gamma\delta_j = -R[x_j](t)$. However, this ODE is itself generally oscillatory, with an unknown initial condition needed to achieve a nonoscillatory solution. Yet if δ_j is nonoscillatory, the first term δ'_j is a factor $x_j = \mathcal{O}(\omega)$ smaller than the second term, thus one might hope that by dropping it a useful reduction in residual might still result. This leads to the algebraic formula $2(x_j(t) + \gamma(t))\delta_j(t) = -R[x_j](t)$ which is solved pointwise for each t . Updating via $x_{j+1} = x_j + \delta_j$ explains our proposed (13). This is a type of defect correction scheme [9]. If ω is a smooth function, then the result is nonoscillatory by construction, without explicit reference to an initial condition.

The early iterates of (12)–(13) illustrate the residual reduction (we give the case $\gamma(t) \equiv 0$, for simplicity, but the results hold for the general case):

$$\begin{aligned} x_0 &= i\omega, & R[x_0] &= i\omega' = \mathcal{O}(\omega), \\ x_1 &= i\omega - \frac{\omega'}{2\omega}, & R[x_1] &= -\frac{\omega''}{2\omega} + \frac{3\omega'^2}{4\omega^2} = \mathcal{O}(1), \\ x_2 &= i\omega - \frac{\omega'}{2\omega} + \delta_1, \text{ where } \delta_1 = \frac{\frac{\omega''}{2\omega} - \frac{3\omega'^2}{4\omega^2}}{2i\omega - \frac{\omega'}{\omega}}, & R[x_2] &= \delta'_1 + \delta_1^2 = \mathcal{O}(\omega^{-1}). \end{aligned} \quad (14)$$

Here our somewhat loose asymptotic notation $\mathcal{O}(\omega)$, *etc.* has meaning over some interval where ω does not change much, *i.e.* that its upper and lower bounds are of the same order. Also, since ω is assumed smooth, we have that ω' , ω'' , *etc.* are of the same order as ω . If we were to include γ , we would assume $\gamma = \mathcal{O}(1)$ and that its derivatives are of the same order as γ itself due to smoothness. This suggests that each iteration reduces the residual by a factor $\mathcal{O}(\omega)$ but brings in one extra derivative of ω (and γ). To verify this pattern for arbitrary j , notice that

$$R[x_{j+1}] = R[x_j] + 2(x_j + \gamma)\delta_j + \delta_j^2 + \delta'_j = \delta_j^2 + \delta'_j,$$

where the first two terms canceled by design, due to (13). Substituting $\delta_j = -R[x_j]/2(x_j + \gamma)$ and using the quotient rule then proves the following useful update for the residual function.

Proposition 1. *Let x_j , ω and γ be smooth functions on an interval on which $x_j + \gamma$ is nonvanishing. Let x_{j+1} be given by the iteration (13). Then the associated residual function (11) obeys the iteration*

$$R[x_{j+1}] = \frac{1}{2(x_j + \gamma)} \left(\frac{(x_j + \gamma)'}{x_j + \gamma} R[x_j] - R[x_j]' \right) + \left(\frac{R[x_j]}{2(x_j + \gamma)} \right)^2. \quad (15)$$

Thus, if one can show that $|x_j + \gamma|$ is uniformly bounded from below by an $\mathcal{O}(\omega)$ constant, and that the final quadratic term in (15) is small, then one might hope that the residual is an asymptotic series shrinking like $R[x_j] = \mathcal{O}(\omega^{1-j})$ for $j = 0, 1, \dots$. However, it will turn out that this series, and

the iteration (13) for x_j , are not convergent: for a typical fixed functions $\omega(t)$ and $\gamma(t)$, the increasing order of derivatives eventually lead to divergence. Nevertheless, the iteration is useful numerically, since when ω varies only a small amount over an interval, the residual decays geometrically for the first few iterations with a rate that improves with larger ω . We will show this rigorously for the case of analytic ω and γ in [Theorem 4](#).

2.2 Discretization of Riccati defect correction

We now turn to the numerical discretization of the iteration (12)–(13) on an interval $[t_i, t_i + h]$ corresponding to the i th time-step of the solver. For now, assume that h is sufficiently small that the functions ω , γ , x_j , R_j , and their first few derivatives are accurately represented by function values on a single $(n + 1)$ -node Chebyshev grid. We will explain our choice of h in [Section 2.6.1](#). The remaining tasks are numerical differentiation of the function x_j needed to evaluate R_j in (11), and numerical quadrature (since $u(t) = \exp \int^t x(\sigma) d\sigma$).

Recall that on the standard interval $[-1, 1]$ the $n + 1$ Chebyshev nodes are $\tilde{\tau}_l = \cos(l\pi/n)$, $l = 0, 1, \dots, n$. In our experiments we fixed $n = 16$, which we found gave a good compromise between very high order and speed of numerical linear algebra. The standard $(n + 1) \times (n + 1)$ differentiation matrix \tilde{D}_n is filled according to [\[53, Ch. 6\]](#). Rescaling to the time-step interval $[t_i, t_i + h]$ gives nodes

$$\tau_l = t_i + \frac{h}{2}[1 + \cos(l\pi/n)], \quad l = 0, 1, \dots, n, \quad (16)$$

and the rescaled matrix $D_n = (2/h)\tilde{D}_n$. Then given a vector $\mathbf{x} \in \mathbb{C}^{n+1}$ with components $x_l := \{x(\tau_l)\}$ values of a smooth function x at the nodes, $D_n \mathbf{x}$ is a vector of approximate derivatives at these nodes. We then fill the vectors of values $\omega_l = \omega(\tau_j)$ and $\gamma_l = \gamma(\tau_j)$. The discretization of the iteration (12)–(13) gives the sequence $\mathbf{x}^{(0)}, \mathbf{x}^{(1)}, \dots, \mathbf{x}^{(k)}$ whose components $l = 0, \dots, n$ obey

$$x_l^{(0)} = i\omega_l, \quad x_l^{(j+1)} = x_l^{(j)} - \frac{R_l^{(j)}}{2(x_l^{(j)} + \gamma_l)}, \quad \text{where } R_l^{(j)} = \sum_{m=0}^n (D_n)_{lm} x_m^{(j)} + [x_l^{(j)}]^2 + 2\gamma_l x_l^{(j)} + \omega_l^2.$$

We postpone choice of the stopping point k to [Section 2.6.3](#).

Finally, we must discretize the antiderivative operation giving $z(t)$ on the interval such that $z' = x$, to then recover a solution $u = e^z$. If dense output is required, *i.e.* the solver is to perform interpolation and compute the numerical solution between internal time nodes, then this is done by constructing the integration matrix Q_n mapping function values at n Chebyshev nodes to values of the antiderivative of the interpolating polynomial at those points (with the last value being zero). We use `chebfun`'s [\[19, 32\]](#) implementation which constructs Q_n as $Q_n = T_n B_n T_n^{-1}$, where T_n and T_n^{-1} convert Chebyshev interpolation polynomial coefficients to node values and vice versa, and B_n is the appropriate Vandermonde matrix. $T_n (T_{n-1})$ is equivalent to the (inverse) discrete cosine transform [\[26, 27\]](#). The matrix Q_n is computed once and for all at $\mathcal{O}(n \log n)$ cost, then at each timestep $Q_n \mathbf{x}$ is performed, followed by a rescaling by $h/2$. If, on the other hand, the solution is required only at the end of the interval, $t = t_1$, then z need not be evaluated at the Chebyshev nodes and it suffices to compute the definite integral $\int_{x_i}^{x_i+h} x dt$ at each timestep. This is done by Clenshaw–Curtis quadrature, following [\[53, Chapter 12\]](#).

2.3 Numerical demonstration of Riccati defect correction

At this point it is useful to illustrate the residual reduction with an example. In the left panel of [Fig. 1](#), we apply the above numerically-discretized iteration to the equation

$$u'' + \omega^2(t)u = 0, \quad \omega(t) = \frac{\sqrt{m^2 - 1}}{1 + t^2}, \quad (17)$$

over a single timestep interval $t \in [0, 0.5]$ covered by a $n = 16$ Chebyshev grid. This choice of $\omega(t)$ is analytic in the neighborhood of the interval, having poles at $\pm i$. For various fixed choices of m , which controls the maximum frequency according to $\omega_{\max} := \sqrt{m^2 - 1}$, we plot the maximum magnitude residual vector $\max_{0 \leq l \leq n} |R_l^{(j)}|$ at the nodes, as a function of iteration number j . We observe that the residual indeed drops geometrically for the first few iterations, with a rate well described by $(\omega_{\max})^{-j}$. Thus, at very large $\omega_{\max} \approx 10^4$ the convergence is extremely rapid, with machine precision reached at $j = 5$. However, for a small $\omega_{\max} = 10$, the iteration suddenly starts diverging beyond 6 iterations, so that only about 5 digits of accuracy can be achieved by optimal stopping. While divergence is to be expected since the series generated by the iteration is asymptotic rather than convergent, one would expect (as in [Section 3](#)) the divergent iteration to be $\mathcal{O}(\omega_{\max})$. Yet, curiously, for other intermediate ω_{\max} values a sudden deterioration of rate (“kink”) occurs also at the *same* $j = 6$. This suggests that the rate change comes from the same mechanism, one unrelated to asymptotic divergence.

We now discuss the cause of this kink phenomenon. With asymptotics ruled out, one might well then suspect discretization error: the action of the matrix D_n does not give the true derivative at the nodes, and this compounds with each iteration. However, the right panel of [Fig. 1](#) provides strong evidence for a third explanation: the amplification of rounding errors. The case of constant $\omega(t)$ provides a convenient diagnostic: since its Riccati residual is zero in exact arithmetic (both in the continuous and discrete cases), only rounding error remains. This error model is shown by the new dotted curves in the plot: they clearly show that the kink occurs when rounding error dominates. Here we picked the value of the constant to be the minimum of $\omega(t)$ in [\(17\)](#) over the interval $t \in [0, 0.5]$, since, for fixed n and h , smaller values of constant ω result in larger discretization errors after $j > 1$ iterations. We suspect that the constancy with ω_{\max} of the kink location j is due to the difference in rounding error slope vs residual reduction slope (on the semi-log plot) being a constant controlled only by the largest eigenvalue of D_n . We find that the position of the kink is determined by a number of parameters, including: the ratio of the distance to the nearest pole of ω and the stepsize h ; the number of nodes n ; and the magnitude of ω . Detailed investigations are deferred to future work.

Remark 2. In [Section 3.1](#) we will show that, in exact arithmetic, even though the number of iterations k required to reach minimal residual grows as $\mathcal{O}(\omega)$, in practice a larger ω requires fewer iterations to reach a fixed accuracy threshold ε . Indeed, solving $\varepsilon \approx \omega^{-k}$ gives a heuristic $k_\varepsilon \approx \log(1/\varepsilon)/\log \omega$.

2.4 Matching Riccati timestep intervals

So far we have explained how to numerically solve for one approximate nonoscillatory Riccati phase function over one timestep $[t_i, t_i + h]$, in the sense of having uniformly small residual on its grid nodes. However, this cannot match general initial conditions $u(t_i)$ and $u'(t_i)$, as needed for a second order ODE timestepper. Yet, the asymptotic iteration [\(13\)](#) can be initialized with $x_0(t) = +i\omega(t)$ (as done in [\(12\)](#)), or with $x_0(t) = -i\omega(t)$. The two resulting Riccati solutions, $x_\pm(t)$, give two linearly independent approximate solutions of the desired ODE [\(1\)](#), namely

$$u_\pm(t) = e^{\int_{t_i}^t x_\pm(\sigma) d\sigma}. \quad (18)$$

Since ω and γ are real, u_+ and u_- are complex conjugates. They may be linearly combined to match any set of complex-valued initial conditions,

$$u(t) = A_+ u_+(t) + A_- u_-(t), \quad t \in [t_i, t_i + h], \quad (19)$$

$$u'(t) = A_+ u'_+(t) + A_- u'_-(t), \quad t \in [t_i, t_i + h], \quad (20)$$

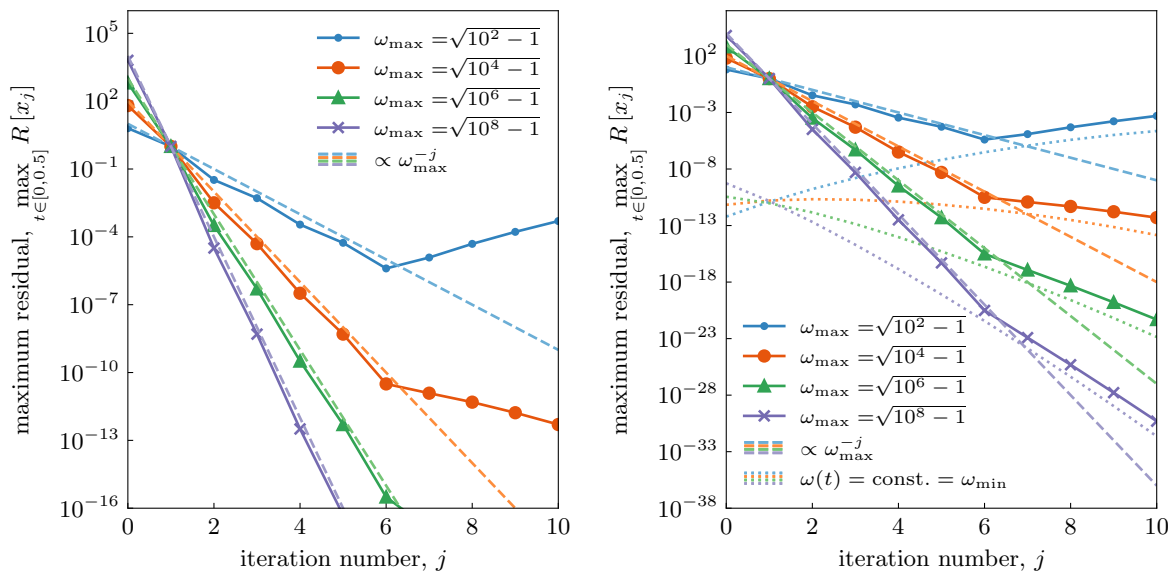


Figure 1: Demonstrations of Riccati residual defect correction. In detail, the left plot shows the maximum magnitude of the residual of the Riccati ODE (11) over the $n = 16$ Chebyshev grid, as a function of iteration count, for the example in Section 2.3. For small ω_{\max} an initial geometric decay eventually becomes unstable growth for large j . The dotted lines show $(\omega_{\max})^{-j}$. The right plot contains the same information as the left plus a set of dotted lines showing our model of roundoff error amplification in the discretized Riccati iteration, computed by setting ω to be constant (see text). The “kink” at $j = 6$ is explained by this error becoming dominant.

with coefficients A_{\pm} satisfying the 2×2 linear system

$$\begin{bmatrix} 1 & 1 \\ x_+(t_i) & x_-(t_i) \end{bmatrix} \begin{bmatrix} A_+ \\ A_- \end{bmatrix} = \begin{bmatrix} u(t_i) \\ u'(t_i) \end{bmatrix}. \quad (21)$$

Here we used that $u_{\pm}(t_i) = 1$ and $u'_{\pm}(t_i) = x_{\pm}(t_i)$ by construction of (18).

2.5 Direct spectral solution on nonoscillatory intervals

If the solution is nonoscillatory, or the asymptotic expansion fails to converge before the residual reaches a user-specified tolerance ε , the solver switches to a standard spectral collocation method on a Chebyshev grid. This achieves an arbitrarily high order timestep in a simple manner. (We note that in other applications a *global* spectral grid is advantageous [53]; here, since adaptive switching and efficiency are needed, integration is best performed over many timestep intervals with a fixed high order grid on each.) Using the Chebyshev nodes $\{\tau_l\}_{l=0}^n$ and differentiation matrix D_n from Section 2.2, Eq. (1) may then be discretized over the interval $t \in [t_i, t_i + h]$ by the linear system

$$F_n \mathbf{u} := (D_n^2 + 2\text{diag}(\{\gamma_l\})D_n + \text{diag}(\{\omega_l^2\})) \mathbf{u} = \mathbf{0}, \quad (22)$$

where $\mathbf{u} := \{u(\tau_l)\}_{l=0}^n$ is the node value vector, and diag indicates the diagonal matrix constructed from a vector. One must also enforce initial conditions via

$$u_n = u(t_i), \quad (D_n \mathbf{u})_n = u'(t_i). \quad (23)$$

Stacking these conditions as rows gives the overdetermined $(n + 3) \times (n + 1)$ linear system

$$\begin{bmatrix} F_n \\ (D_n)_{n,:} \\ (\mathbb{I}_n)_{n,:} \end{bmatrix} \mathbf{u} = \begin{bmatrix} \mathbf{0}_n \\ u'(t_i) \\ u(t_i) \end{bmatrix}, \quad (24)$$

which is solved in the least-squares sense via SVD with $\mathcal{O}(n^3)$ cost. $u(t)$ at the interval's upper end can be read off as the first element (since nodes τ_l are ordered backwards) of the solution vector \mathbf{u} , and its derivative as the first element of $D_n \mathbf{u}$. These then serve as the initial conditions for the subsequent time-step.

We estimate the error induced over this timestep $[t_i, t_i + h]$ by comparing to the solution at the interval endpoint using a doubled value of n . If the relative difference falls below the user-specified threshold ε , the step with doubled n is accepted (t_i is advanced by h). Otherwise the timestep is rejected (t_i is unchanged), and the algorithm repeats with h halved. Computation time spent in failed steps is lost, making it imperative that the initial stepsize estimate h is chosen carefully. We describe the procedure for choosing h for both spectral and asymptotic steps in detail in the next section.

2.6 Adaptive selection of interval size and type

In this section we explain the adaptive stepsize and method-switching algorithm. The left side of [Fig. 2](#) shows a summary flowchart.

2.6.1 Initial stepsize estimates

At each timestep start t_i , a decision needs to be made about whether to use the Riccati defect correction or the Chebyshev spectral method. Both types of steps could be attempted and the decision based upon their estimated error (as done in [\[2\]](#)). Instead, we find it more efficient to use local properties of ω at t_i to get initial stepsize estimates. Recalling [\(14\)](#), the first correction term is ω'/ω , giving the approximate timescale

$$h_{\text{osc}} = \frac{\omega(t_i)}{\omega'(t_i)}. \quad (25)$$

[Theorem 4](#) will also support this by showing that the ratio of bounds on ω' and ω appears in the rate of convergence of successive Riccati residuals. In practice to approximate $\omega'(t_i)$, we use Chebyshev differentiation from the grid of the previous timestep, and from the grid of an initial stepsize at $t = t_0$, supplied by the user.

A similar estimate for the spectral method should depend on two things: how oscillatory the solution is, and on what timescales the coefficients in [\(1\)](#) change, *i.e.* their smoothness. Using the former as our criterion, a measure of the rate of oscillations is simply the frequency, giving the timescale

$$h_{\text{slo}} = \frac{1}{\omega(t_i)}. \quad (26)$$

These initial stepsize estimates are too crude to use directly, since ω , ω' , or γ may change significantly over such an interval. Nonetheless they provide a useful starting point for refinement.

2.6.2 Refining the stepsize estimates

The discretization used in the Riccati defect correction method in [Section 2.2](#) is certainly no more accurate than the error in which the coefficient functions ω and γ are represented on the Chebyshev grid. Therefore we estimate their Chebyshev interpolation error as follows. Let $\mathbf{f} \in \mathbb{R}^{n+1}$ indicate

the vector of nodes values $\{f(\tau_l)\}$ for a function f which will be either ω or γ . Let $f^*(t)$ be the Lagrange polynomial interpolant through the nodes $\{\tau_l\}_{l=0}^n$. Let $\tau_l^* := t_i + \frac{h}{2}[1 + \cos(l\pi/n + \pi/(2n))]$, $l = 0, \dots, n-1$ be the set of n points that lie halfway in between the $n+1$ Chebyshev nodes on the unit half-circle. Then define the error estimate

$$\Delta_n[f] := \max_{l=0,1,\dots,n} \left| \frac{f(\tau_l^*) - f^*(\tau_l^*)}{f(\tau_l^*)} \right|. \quad (27)$$

Since $\{f^*(t_l^*)\} = L_n \mathbf{f}$ for some interpolation matrix L_n that is independent of the interval choice, in practice L_n is computed only once, *e.g.* by solving a Vandermonde system in a backwards stable fashion. (Even though such a system is exponentially ill-conditioned, the interpolation itself is very accurate up to $n \lesssim 40$ for Chebyshev nodes; see [36, Appendix A].)

Letting Δ denote the larger of $\Delta_n[\omega]$ and $\Delta_n[\gamma]$, we accept or update the stepsize as follows,

$$h \leftarrow \begin{cases} h & \text{if } \Delta \leq \varepsilon_h, \\ \min \left(0.7h, 0.9h \left(\frac{\varepsilon_h}{\Delta} \right)^{\frac{1}{n+1}} \right) & \text{otherwise,} \end{cases} \quad (28)$$

where ε_h is a parameter quantifying relative tolerance (distinct from ε). In the above, the $1/(n+1)$ exponent is justified by noting that the error in $(n+1)$ -point Chebyshev interpolation is proportional to h^{n+2} , therefore if Δ exceeds ε_h , using an exponent slightly larger than $1/(n+2)$ takes the local error back down to a value smaller than ε_h , which is further ensured by multiplying by the safety factor 0.9. We decrease the step to $0.7h$ if it yields a smaller stepsize to ensure quicker convergence if Δ is only slightly larger than ε_h . The factors 0.7 and 0.9 were set based on empirical tests.

The local error of Chebyshev spectral steps depends on both the stepsize and the number of nodes. Since within a step we iterate over both of these until convergence, we only need to ensure that over our proposed stepsize the timescale over which u changes ($\approx 1/\omega$) does not increase too much. Starting from $h = h_{\text{slo}}$, we refine the stepsize proposal according to

$$h \leftarrow \begin{cases} h/2 & \text{if } \min_{j=0,1,\dots,n} \frac{1}{\omega(t_j^*)} < \sigma h \\ h & \text{otherwise,} \end{cases} \quad (29)$$

with $\sigma = 0.8$ chosen experimentally.

2.6.3 Choosing the step type

With a refined h_{osc} and h_{slo} in hand, we can make an informed decision about which type of step to take.

Proposition 3. *Let h_{osc} and h_{slo} be the refined stepsize proposals for a step to be taken from $t = t_i$ using the asymptotic expansion and the Chebyshev spectral method, respectively. The algorithm chooses to attempt an asymptotic step of size h_{osc} if and only if*

$$h_{\text{osc}} > 5h_{\text{slo}} \quad \text{and} \quad \omega(t_i)h_{\text{osc}} > 2\pi,$$

otherwise it will attempt a spectral step of size h_{slo} .

The reason behind requiring the proposed stepsize for an asymptotic step not to simply be larger than that of a Chebyshev spectral step is that in regions where the two stepsizes compete, the asymptotic method rarely converges before the residual reaches ε , either because ω is not large enough, or either of γ and ω' is too large. The prefactor of 5 was set based on numerical experiments.

If an asymptotic step was decided to be attempted, the algorithm will start iterating over x_j according to (13), while monitoring the maximum residual over the nodes. If $\max_{l=0,\dots,n} |R[x_j](\tau_l)| < \varepsilon$ or $\max_{l=0,\dots,n} |R[x_j](\tau_l)| \geq \max_{l=0,\dots,n} |R[x_{j-1}](\tau_l)|$, the iteration is stopped. In the former case,

the proposed solution $u(t_i + h)$ is accepted and the independent variable is incremented, $t := t_i + h$. Otherwise, the step is retried with size $h = h_{\text{slo}}$ using the spectral method.

If either of the conditions in [Proposition 3](#) were not met, a spectral step is attempted with $h = h_{\text{slo}}$. The local error of the step is then estimated and the number of nodes, as well as the stepsize, is adapted until a local error value of at most ε is reached, as described in [Section 2.5](#).

We summarize the entire adaptive switching algorithm in the left panel of [Fig. 2](#).

3 Error analysis for the Riccati iteration

Here we prove our main rigorous result: the defect correction of [Section 2.1](#) in the case of analytic coefficients induces temporary geometric decrease of the Riccati residual by a factor $\mathcal{O}(\omega)$ per iteration. Indefinite geometric decrease is not in general possible because of factorial growth due to repeated differentiation; the iteration is asymptotic in $\omega \gg 1$, but not convergent. We abbreviate the residual function by $R_j = R_j(t) := R[x_j](t)$. Our main tools in proving the following will be [Proposition 1](#) (the iteration for R_j), induction, and complex analysis.

Theorem 4. *Fix $t \in \mathbb{R}$, and let the frequency function ω and damping function γ be analytic in the closed ball $B_\rho(t) := \{z \in \mathbb{C} : |z - t| \leq \rho\}$, for some $\rho > 0$, with the bounds in this ball*

$$\eta_1 \leq |\omega(z)| \leq \eta_2, \quad (30)$$

$$|\omega'(z)| \leq \eta_3 \leq \frac{\eta_1^2}{17}, \quad (31)$$

$$|\gamma(z)| \leq \eta_4 \leq \frac{\eta_1^2}{34\eta_2}. \quad (32)$$

Let the nonnegative integer k be small enough that

$$r := \frac{1}{2\tilde{\eta}_1\rho} \left(1 + \frac{\tilde{\eta}_2}{\tilde{\eta}_1} \right) k + \frac{\tilde{\eta}_3}{4\tilde{\eta}_1^2} \leq \frac{3}{4}, \quad (33)$$

where

$$\tilde{\eta}_1 = \eta_1 - \eta_4 - \frac{17\tilde{\eta}_3}{4\eta_1}, \quad (34)$$

$$\tilde{\eta}_2 = \eta_2 + \eta_4 + \frac{17\tilde{\eta}_3}{4\eta_1}, \quad (35)$$

$$\tilde{\eta}_3 = \eta_3 + 2\eta_2\eta_4. \quad (36)$$

Then after any number $j \leq k$ of iterations of [\(12\)–\(13\)](#), the function x_j has Riccati residual [\(11\)](#) bounded at the point t by

$$|R_j(t)| \leq \tilde{\eta}_3 r^j. \quad (37)$$

This shows, for ω' and γ sufficiently small, temporary geometric convergence up to k iterations, but at a rate r that deteriorates with k . For any k to satisfy [\(33\)](#), ω must have a sufficiently large lower bound η_1 , *i.e.* t must be in a sufficiently oscillatory region for the original ODE. The condition [\(31\)](#) on ω' is similar to that in WKB: the *relative ω change per period* should be less than some small constant.

Remark 5. *By construction, $[\tilde{\eta}_1, \tilde{\eta}_2]$ is only a limited expansion of the interval $[\eta_1, \eta_2]$ containing the range of $|\omega|$ in the ball. In particular, by the inequalities [\(30\)–\(32\)](#) and definitions [\(34\)–\(36\)](#), $\tilde{\eta}_1 \geq 8\eta_1/17$ and $\tilde{\eta}_2 \leq \eta_2 + 9\eta_1/17$. Applying this we see that the last term in the definition of r in [\(33\)](#) is no more than $17/128 \leq 0.14$, thus can at worst cause only modest deterioration in the rate.*

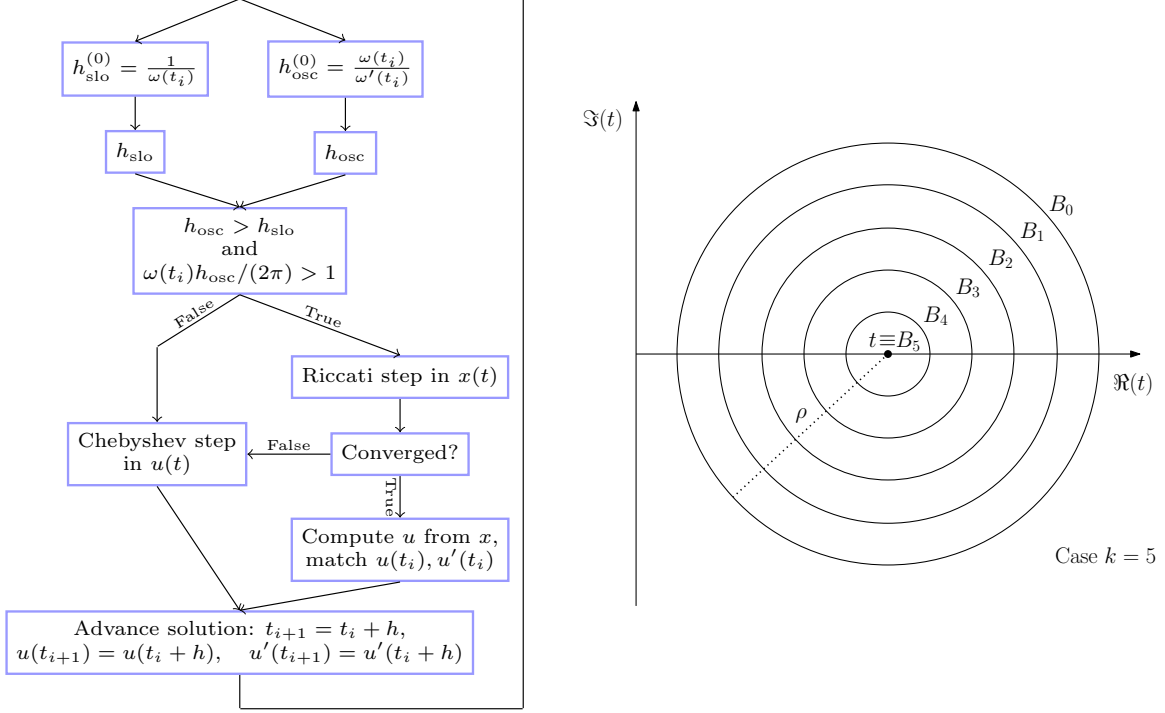


Figure 2: Left: Flowchart showing choice of stepsize h and step type (Riccati vs standard Chebyshev) for our proposed algorithm. t_i is the start of the current timestep. Right: Sketch of a nested equispaced set of balls centered on the target time t , used in the proof of [Theorem 4](#).

Remark 6. *In the limit when ω tends to be constant in the ball (η_3 small) and damping is small (η_4 small), then the geometric rate r tends to $k/\omega\rho$, where we can interpret $\omega\rho$ as 2π times the number of oscillation periods across the ball radius. Then, for example, with a radius of only 5 periods, r satisfies (33) for $k \leq 25$.*

Proof. Define the concentric nested set of closed balls $B_j := B_{\rho_j}(t)$, with radii $\rho_j := (1 - j/k)\rho$, $j = 0, 1, \dots, k$. Note that B_0 is the original ball in the statement of the theorem, while $B_k = \{t\}$ is the single point of interest; see the right panel of [Fig. 2](#). For any function f analytic in B_j we abbreviate its ∞ -norm by $\|f\|_j := \max_{z \in B_j} |f(z)|$. We will bound f' in B_{j+1} in terms of $\|f\|_j$ by applying Cauchy's theorem for derivatives [52],

$$f'(z) = \frac{1}{2\pi i} \int_{|\zeta-t|=\rho_j} \frac{f(\zeta) d\zeta}{(\zeta-z)^2}, \quad z \in B_{j+1}. \quad (38)$$

Bounding the integrand, then using the cosine rule we get

$$|f'(z)| \leq \frac{\|f\|_j}{2\pi} \int_{|\zeta-t|=\rho_j} \frac{|d\zeta|}{|\zeta-z|^2} = \frac{\|f\|_j}{2\pi} \int_0^{2\pi} \frac{\rho_j d\theta}{|z|^2 + \rho_j^2 - 2|z|\rho_j \cos \theta}.$$

We now use $\int_0^{2\pi} d\theta/(a + b \cos \theta) = 2\pi/\sqrt{a^2 - b^2}$ for $b < a$ [28, Eq. 3.613.1], with $a = |z|^2 + \rho_j^2$ and $b = -2|z|\rho_j$, so that $\sqrt{a^2 - b^2} = \rho_j^2 - |z|^2$. Noting that the case $|z| = \rho_{j+1}$ bounds the others, and using $\rho_j = (1 - j/k)\rho$, we compute, for any $0 \leq j < k$,

$$\|f'\|_{j+1} \leq \frac{\|f\|_j}{2\pi} \frac{2\pi\rho_j}{\rho_j^2 - \rho_{j+1}^2} = \frac{\|f\|_j}{2\rho} \frac{k(k-j)}{2k-2j-1} = \frac{\|f\|_j}{2\rho} k \left[\frac{1}{2} + \frac{1}{2(2k-2j-1)} \right] \leq \frac{k}{\rho} \|f\|_j. \quad (39)$$

Note that this bound is a factor $\mathcal{O}(k)$ better than naively lower bounding the denominator in (38).

We now use induction in iteration number j . We take as the induction hypothesis that x_ℓ (and thus R_ℓ) is analytic in B_j , for all $0 \leq \ell \leq j$, with

$$\tilde{\eta}_1 \leq |x_\ell + \gamma| \leq \tilde{\eta}_2 \quad \text{in } B_j, \quad \text{for all } \ell = 0, 1, \dots, j, \quad (40)$$

$$|R_\ell| \leq \tilde{\eta}_3 r^\ell \quad \text{in } B_j, \quad \text{for all } \ell = 0, 1, \dots, j, \quad (41)$$

where r is defined by (33). Assuming for now the hypothesis for j , we apply simple bounds to the residual iteration (15), lower-bounding denominator magnitudes and upper-bounding numerators via (40), and applying (39) to the two derivative terms, to get

$$\|R_{j+1}\|_{j+1} \leq \frac{1}{2\tilde{\eta}_1} \left(\frac{1}{\tilde{\eta}_1} \frac{k}{\rho} \tilde{\eta}_2 + \frac{k}{\rho} \right) \|R_j\|_j + \left(\frac{\|R_j\|_j}{2\tilde{\eta}_1} \right)^2 \leq r \cdot \|R_j\|_j \leq \tilde{\eta}_3 r^{j+1},$$

where in the middle step we used the crude bound $\|R_j\|_j \leq \tilde{\eta}_3$ following from (41) and that $r \leq 1$, and then the definition of r in (33). The lower cases $\ell \leq j$ follow trivially from the hypothesis since the balls are nested. Thus (41) is proven for $j+1$.

It remains to verify that (40) also holds for $j+1$. By the functional iteration (12)–(13),

$$x_{j+1}(z) + \gamma(z) = i\omega(z) + \gamma(z) - \sum_{\ell=0}^j \frac{R_\ell(z)}{2(x_\ell(z) + \gamma(z))}, \quad z \in B_{j+1}.$$

Using the hypothesis, the sum is pointwise bounded in magnitude in B_{j+1} by

$$\left| \sum_{\ell=0}^j \frac{R_\ell}{2(x_\ell + \gamma)} \right| \leq \frac{\tilde{\eta}_3}{2\tilde{\eta}_1} \cdot \sum_{\ell=0}^j r^\ell \leq \frac{\tilde{\eta}_3}{2\tilde{\eta}_1} \cdot 4,$$

where the upper bound in (33) was used to bound the geometric series. Using (34) for $\tilde{\eta}_1$ and (36) for $\tilde{\eta}_3$ we write this upper bound as

$$\left| \sum_{\ell=0}^j \frac{R_\ell}{2(x_\ell + \gamma)} \right| \leq 2 \frac{\eta_3 + 2\eta_2\eta_4}{\eta_1 - \eta_4 - \frac{17\eta_3}{4\eta_1} - \frac{17\eta_2\eta_4}{2\eta_1}},$$

then extend it by lower-bounding the denominator via (31) and the crude bound $\eta_4 \leq \eta_1/34$ from (32). This gives

$$\left| \sum_{\ell=0}^j \frac{R_\ell}{2(x_\ell + \gamma)} \right| \leq \frac{17\eta_3}{4\eta_1} + \frac{17\eta_2\eta_4}{2\eta_1},$$

which, when combined with $|\omega| \leq \eta_2$ and $|\gamma| \leq \eta_4$ yields

$$\|x_{j+1} + \gamma\|_{j+1} \leq \eta_2 + \eta_4 + \frac{17\eta_3}{4\eta_1} + \frac{17\eta_2\eta_4}{2\eta_1} = \tilde{\eta}_2,$$

verifying the upper bound (40) for $j+1$. Instead combining with $|\omega| \geq \eta_1$ gives

$$|x_{j+1}| \geq \eta_1 - \eta_4 - \frac{17\eta_3}{4\eta_1} - \frac{17\eta_2\eta_4}{2\eta_1} = \tilde{\eta}_1$$

in B_{j+1} , which verifies the lower bound (40). Again, the hypothesis is inherited for $\ell \leq j$ by the nesting of the balls.

Finally, the base case $j=0$ for induction satisfies (40)–(41) by the conditions of the theorem, since $x_0(t) = i\omega(t)$, noting $[\eta_1, \eta_2] \subset [\tilde{\eta}_1, \tilde{\eta}_2]$, while $R_0(t) = i(\omega'(t) + 2\gamma\omega)$ is bounded in magnitude by $\tilde{\eta}_3$. \square

In the above theorem, the choice of $3/4$ in (33) was merely a convenient one, chosen so that the bounds $[\tilde{\eta}_1, \tilde{\eta}_2]$ on $|x_j + \gamma_j|$ involving the geometric sum were not much wider than the bounds $[\eta_1, \eta_2]$ on $|\omega|$. Note that in the case of $\gamma \equiv 0$ it is possible to simplify the statement and proof of the theorem somewhat, and improve some of the constants.

3.1 Practical aspects of residual reduction

The fact that, as k grows, the rate r bound in Theorem 4 deteriorates, we believe to be an inevitable consequence of the series generated by the iteration being asymptotic in $1/\omega$ but not in general convergent. However, given a function $\omega(t)$ uniformly large enough in a ball, by stopping at a roughly optimal k (an idea called “superasymptotics” [8, 10]) one can achieve exponential convergence with respect to the size of the frequency ω , as follows.

Corollary 7 (Superasymptotic approximation). *Suppose ω and γ satisfy the conditions (30)–(32) about a point $t \in \mathbb{R}$, and let $\alpha := (1 + \tilde{\eta}_2/\tilde{\eta}_1)/2\tilde{\eta}_1\rho$ be the first term in the rate (33) arising from these bounds. Then there is a nonnegative integer k such that*

$$|R_k(t)| \leq e\tilde{\eta}_3 e^{-1/5\alpha}.$$

Proof. Set k to be the integer in the interval $[1/5\alpha - 1, 1/5\alpha]$. Then since the final term in (33) is bounded by $17/128 \leq 0.14$ by Remark 5, and the first term is $k\alpha \leq 1/5$, we get $r \leq e^{-1}$, which is also $\leq 3/4$ so that (37) holds. Choosing $j = k$, and inserting the lower bound on k , $|R_k(t)| \leq \tilde{\eta}_3 r^k \leq \tilde{\eta}_3 e^{-(1/5\alpha - 1)}$, which finishes the proof. \square

Recalling that $\alpha = \mathcal{O}(1/\omega)$, this shows that an ω -dependent number of iterations can give, in exact arithmetic, an exponentially convergent pointwise residual,

$$|R(t)| = \mathcal{O}(e^{-c\omega})$$

for some constant $c > 0$. In the limit where ω tends to constant in the ball of radius ρ about t , then α tends to $1/\omega\rho$, so the above constant is roughly $c \approx \rho/3$. Equivalently, roughly one decimal digit is achieved per 1.1 periods of oscillation across the ball radius.

However, this optimal number of iterations grows as $k = \mathcal{O}(\omega)$, so for large ω is impractical, and unnecessary. In practice we use the adaptive residual stopping criterion for k described in Section 2.6.3. By returning to Theorem 4 and dropping the small second term in (33) we get, in the limit of constant ω in the ball,

$$|R_k(t)| \approx \tilde{\eta}_3 \left(\frac{k}{\rho\omega} \right)^k.$$

This shows *nearly* geometric convergence in k , sufficient to reach machine accuracy efficiently with a few iterations when ω is large. For large $\rho\omega$ one may approximately invert this to predict the iteration number k sufficient for $|R_k| \approx \varepsilon$, to get $k_\varepsilon \approx \frac{\log \varepsilon^{-1}}{\log \rho\omega}$, a refinement of Remark 2.

Finally we show that the stopping criterion for k based on the absolute residual $R[x_k]$ of the Riccati equation is relevant because this is equal to the *relative residual* of the original ODE.

Proposition 8 (Relationship of residuals). *Let $R[x_k](t)$ be the residual of the Riccati equation as defined in (11). Then if $\tilde{R}[u_k](t)$ is the associated residual of the original ODE (1), defined as*

$$\tilde{R}[u_k](t) := u_k'' + 2\gamma(t)u_k' + \omega^2(t)u_k, \quad (42)$$

for $u_k(t) = e^{\int_0^t x_k(\sigma) d\sigma}$, then

$$\frac{\tilde{R}[u_k](t)}{u_k(t)} = R[x_k](t). \quad (43)$$

Proof. This follows straightforwardly from substitution of the above form of u_k into (42). \square

4 Numerical results

Our numerical experiments will test the integration of 2nd-order linear ODEs that include regions with highly-oscillatory solutions. In such regions the condition number of the problem itself becomes large, and this limits the achievable accuracy of *any* numerical method that works with finite-precision input data. Recall [29, Ch. 6] that the definition of relative condition number for evaluation of a fixed function $f(t)$ is $\kappa(t) := |tf'(t)/f(t)|$. As a toy example, for the oscillatory function $f_{\omega_0}(t) = e^{i\omega_0 t}$, the condition number of evaluating $f_{\omega_0}(1)$ is $\kappa(1) = \omega_0$, the total phase accrued over the interval $[0, 1]$. However, since ω_0 is also an input to this problem, the relative condition number *with respect to variation in ω_0* is also relevant. The latter is $|\omega_0/f_{\omega_0}(1)| \cdot |\partial f_{\omega_0}(1)/\partial \omega_0| = \omega_0$, in this case the same as the condition number with respect to t . Thus, if $\omega_0 = 10^7$, so that $\kappa = 10^7$ by either definition, then using double-precision arithmetic with $\varepsilon_{\text{mach}} \approx 10^{-16}$ no algorithm can achieve an error less than $\mathcal{O}(\kappa \cdot \varepsilon_{\text{mach}}) \approx 10^{-9}$, the error for a backward-stable algorithm.

For more general oscillatory solutions to the IVP (1)–(3), the two above types of condition number generally differ, and the larger controls the minimum achievable error. For example, scaling $\omega(t) = \omega_0 \Omega(t)$ as in Section 1, then taking the zero-order approximation $u(t) = e^{\pm i\omega_0 \int_{t_0}^t \Omega(\sigma) d\sigma}$, we see that its relative condition number with respect to t is $|t\omega(t)|$, determined by the local frequency, whereas with respect to ω_0 it is $\int_{t_0}^t \omega(\sigma) d\sigma$, the total phase accrued over (t_0, t) . The loss in achievable accuracy due to the latter κ is well known, and may be interpreted as inevitable accuracy loss in taking the sine or cosine of the phase function [11]. This motivates the following.

Definition 9 (Condition number and achievable accuracy for an oscillatory region). *Let u be a solution to (1) on (t_0, t_1) of the form $u(t) = e^{z(t)}$ where $\text{Im } z'(t) > 0$ for all $t \in (t_0, t_1)$. We define the condition number of the problem of evaluation of $u(t)$ by*

$$\kappa(t) := \max [|tz'(t)|, \text{Im}(z(t) - z(t_0))] \quad (44)$$

and then the resulting best achievable accuracy using finite precision by

$$\kappa \cdot \varepsilon_{\text{mach}}. \quad (45)$$

In practice we use a numerical phase function solution to estimate κ . In our examples the first (frequency) term does not dominate the second (accrued phase) term. In the case where there is no such global phase function representation $u = e^z$, we estimate this second term by summing the absolute differences in $\text{Im } z$ across the various intervals in each of which a local phase function exists. Note that this definition does not capture additional κ fluctuations inherent in real-valued functions: taking the real part of the toy example, $f_{\omega_0}(t) = \cos \omega_0 t$, κ with respect to t becomes $|t\omega_0 \tan \omega_0 t|$, which fluctuates wildly from 0 to ∞ , although a typical value is again $\mathcal{O}(\omega_0)$.

In the below tests we denote absolute error in a numerical solution by $\Delta u(t) := |u(t) - \tilde{u}(t)|$, where u is a reference solution computed either analytically or by a converged reference solver, and \tilde{u} is the solution given by the method under test.

All computations were performed on an Intel Xeon Gold 6244, 16-core, 3.6 GHz workstation with 264 GB of RAM. No attempt has been made to parallelize our code, and for the sake of fair comparison all experiments were run with a single thread (`OMP_NUM_THREADS=1`). The open-source software implementing the proposed method and the above experiments in Python is available on GitHub⁴. The code relies on the `numpy` [33] and `scipy` [54] packages to perform linear algebra. For the numerical experiments, the following versions of software were used: Python 3.8.12, `numpy` 1.23.1, `scipy` 1.9.3.

⁴<https://github.com/fruzsinaagocs/riccati>

4.1 The Airy equation

A simple but effective test for highly oscillatory solvers is the Airy ODE,

$$u'' + tu = 0, \quad t \in [1, 10^8], \quad (46)$$

with initial conditions

$$u(1) = \text{Ai}(-1) + i\text{Bi}(-1), \quad u'(1) = -\text{Ai}'(-1) - i\text{Bi}'(-1). \quad (47)$$

where Ai, Bi are the Airy functions [17, Chapter 9]. Its unique solution is

$$u(t) = \text{Ai}(-t) + i\text{Bi}(-t). \quad (48)$$

This is challenging for standard numerical methods, due to the growing frequency $\omega(t) = \sqrt{t}$, but is expected to be easy for specialized oscillatory methods since the change in $\omega(t)$ per wavelength becomes arbitrarily small, making an asymptotic approximation (such as WKB) an increasingly good local approximation.

Choosing a tolerance $\varepsilon = 10^{-12}$, Fig. 3 shows the internal steps our numerical solver takes while solving (46)–(47), color-coded by step type, as well as the progression of stepsizes, the numerical relative error function $\Delta u(t)/u(t)$, and number of oscillation periods traversed in a single step, n_{osc} . The stepsize h is expected to reflect the timescale over which ω changes, therefore $h \propto \omega(t)/\omega'(t) \propto t$, which is observed. The numerical error traces the theoretical minimum, $\kappa \cdot \varepsilon_{\text{mach}}$, to within a digit. The number of oscillations traversed per step can be derived from $h(t)$: $n_{\text{osc}} \propto \omega h \propto t^{3/2}$, a result clearly supported by the bottom-right figure panel. Our solver covers around 10^{11} periods using ≈ 30 timesteps, taking ≈ 10 milliseconds of CPU time, while achieving an error around 10^{-11} (or, when larger, the theoretical minimum (45)).

Fig. 4 demonstrates the convergence of our method on the Airy equation for different solution interval lengths, achieved by varying t_1 with $t_0 = 1$ fixed. This shows that the achieved relative accuracy is approximately bounded (within close to one digit of accuracy) by the requested tolerance ε , down to the theoretical minimum error (45).

4.2 Comparison with standard and state-of-the-art oscillatory solvers

Here we compare the performance of the present solver, which we now refer to as adaptive Riccati defect correction (ARDC), to that of the following recent specialized methods for oscillatory ODEs:

Kummer’s phase function method: an arbitrarily high-order solver described by Bremer [11], specifically created for highly oscillatory problems with neither a friction term nor transitions to nonoscillatory behavior. The user provides ω as a function. We use the Fortran 90 implementation provided by its author at <https://github.com/JamesCBremerJr/Phase-functions>

oscode: an adaptive solver which switches from low-order WKB (in oscillatory regions) to Runge–Kutta (in smooth regions) [2, 3], that can accommodate a friction term. It requires only requires the user to specify ω and γ , which can be given as either closed-form functions or as timeseries. The solver has both a Python and C++ interface, but for the experiments below it is called in Python.

The WKB marching method [5, 38]: a solver using the mechanism of [2] to switch between WKB-inspired and Runge–Kutta methods. Its convergence order in the oscillatory regions is one higher than that of `oscocode`, but does not (easily) generalize to include a γ term. It requires the user to provide the derivative functions of ω up to $\omega^{(5)}$. It is implemented in MATLAB.

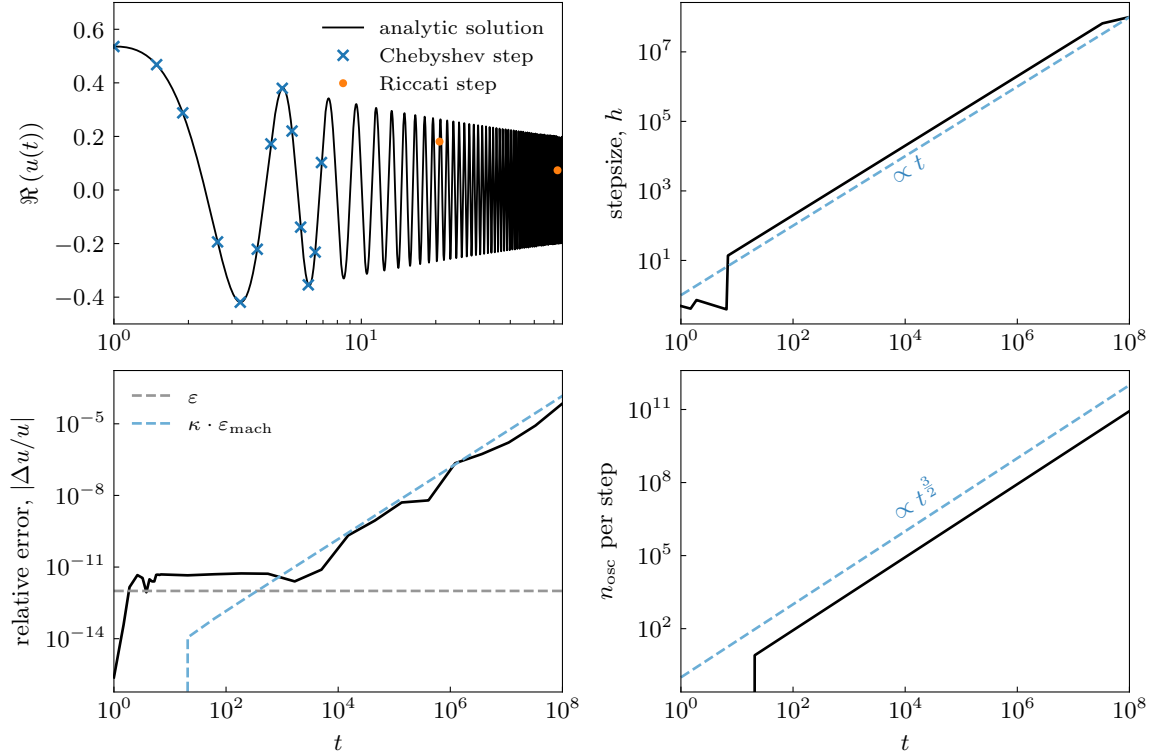


Figure 3: Numerical solution of the Airy equation. The top left panel shows the real part of the analytic solution in black, on top of which the individual timesteps of the solver are plotted, colored by their step type. The top right panel plots the stepsize as a function of time, which exhibits linear growth. The bottom left shows the relative error achieved by the solver in black, with two dashed lines to guide the eye: the chosen solver tolerance ε in gray, and the best achievable accuracy (45) in blue. On the bottom right, we show the number of wavelengths of oscillation traversed in a single step, as a function of time.

As the test problem we take the ODE in [11, Eq. (237)],

$$u'' + \omega^2(t)u = 0, \quad \text{where } \omega^2(t) = \lambda^2(1 - t^2 \cos 3t) \quad (49)$$

on $t \in [-1, 1]$, subject to the initial conditions

$$u(-1) = 0, \quad u'(-1) = \lambda, \quad (50)$$

where we vary the frequency scaling λ between 10 and 10^7 .

For a reference solver we use the Kummer's phase function method with $\varepsilon = 10^{-14}$ (its default tolerance), since it is arbitrarily high order, and exhibited around 13 accurate digits in its published tests at $\lambda = 10$ [11, Table 1]. As expected, the ill-conditioning of the problem as λ grows reduces its accuracy, giving only 8 digits by $\lambda = 10^7$. This is in accordance with the theoretical minimum error (45), thus there will be no meaning given to reported errors below these. Note that conventional solvers are ruled out as a reference since the number of oscillations we test are simply too large.

Table 1 presents the runtime statistics of ARDC, Kummer's phase function method, the WKB marching method, and `oscde` respectively. For all solvers, we set the relative tolerance to $\varepsilon = 10^{-12}$, and in all cases work in double precision. For our solver, we set the number of Chebyshev nodes

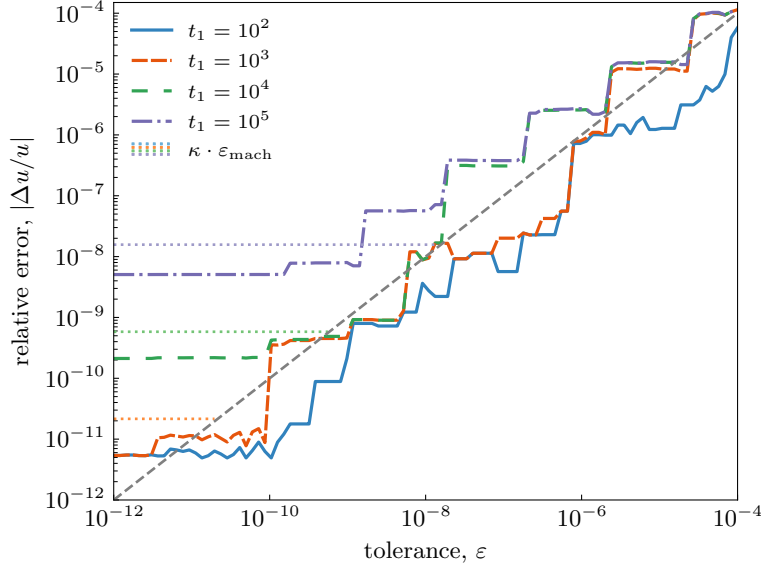


Figure 4: Error performance of the solver when applied to the Airy equation, (46)–(47). The plot shows the achieved relative error of the solver vs the requested tolerance for the example in Section 4.1, while the upper end of the integration interval t_1 is varied. The dotted lines show the theoretical minimum (45) for each interval, which the solver indeed matches within a small constant.

in Riccati (oscillatory) steps (see Section 2.5) to $n = 40$, the tolerance for stepsize selection to $\varepsilon_h = 10^{-13}$, and the number of Chebyshev nodes in the spectral (nonoscillatory) steps to the default $n = 16$. For all other methods, none of the input parameters were modified from their default values with the exception of the local tolerance.

We now describe the quantities tabulated in Table 1:

max $|\Delta u/u|$: Maximum relative error over the integration range, evaluated at the timesteps taken internally by the solver. If less than the error of the reference Kummer method as reported in [11, Table 1], the latter is stated as its upper bound.

t_{solve} : Total runtime, in seconds, of a single ODE solve, averaged over between 10^3 and 10^5 runs. This is equivalent to the “phase function construction time” of [11, Table 1].

$n_{\text{s,osc}}$: Number of time steps of oscillatory type. When this quantity appears as (n_1, n_2) , n_1 denotes the number of attempted steps of the given type, out of which n_2 have been successful (accepted). The same convention applies to $n_{\text{s,slo}}$ and $n_{\text{s,tot}}$.

$n_{\text{s,slo}}$: Number of time steps of “standard” (Runge–Kutta or Chebyshev spectral) type, *i.e.* in the nonoscillatory regions of the solution.

$n_{\text{s,tot}}$: Total number of steps performed by the solver, sum of $n_{\text{s,osc}}$ and $n_{\text{s,slo}}$.

n_f : Total number of function evaluations during a single ODE solve.

n_{LS} : Total number of linear solves performed by ARDC.

Fig. 5 provides a visual comparison of the runtime (left) and achieved relative error (right) as a function of the frequency parameter λ of the solvers being tested. In addition to runtimes and

method	λ	$\max \Delta u/u $	t_{solve}/s	$n_{s,\text{osc}}$	$n_{s,\text{slo}}$	$n_{s,\text{tot}}$	n_f	n_{LS}
ARDC	10^1	2.01×10^{-11}	1.81×10^{-2}	(24, 0)	(24, 24)	(48, 24)	11388	55
	10^2	6.3×10^{-13}	2.42×10^{-3}	(4, 2)	(2, 2)	(6, 4)	1830	5
	10^3	$\leq 3 \times 10^{-12}$	4.70×10^{-4}	(2, 2)	(0, 0)	(2, 2)	732	1
	10^4	$\leq 5 \times 10^{-11}$	4.05×10^{-4}	(2, 2)	(0, 0)	(2, 2)	732	1
	10^5	$\leq 3 \times 10^{-10}$	3.91×10^{-4}	(2, 2)	(0, 0)	(2, 2)	732	1
	10^6	$\leq 5 \times 10^{-9}$	3.79×10^{-4}	(2, 2)	(0, 0)	(2, 2)	732	1
	10^7	$\leq 4 \times 10^{-8}$	3.59×10^{-4}	(2, 2)	(0, 0)	(2, 2)	732	1
Kummer's phase function	10^1	$\leq 7 \times 10^{-14}$	6.74×10^{-3}				75921	
	10^2	$\leq 5 \times 10^{-13}$	3.76×10^{-3}				44054	
	10^3	$\leq 3 \times 10^{-12}$	2.92×10^{-3}				24740	
	10^4	$\leq 5 \times 10^{-11}$	2.74×10^{-3}				20521	
	10^5	$\leq 3 \times 10^{-10}$	3.19×10^{-3}				21808	
	10^6	$\leq 5 \times 10^{-9}$	3.73×10^{-3}				23525	
	10^7	$\leq 4 \times 10^{-8}$	3.18×10^{-3}				22468	
WKB marching	10^1	1.95×10^{-11}	2.39×10^{-1}	0	0	1655	18293	
	10^2	2.78×10^{-10}	3.10×10^0	0	0	16181	179861	
	10^3	$\leq 3 \times 10^{-12}$	1.24×10^0	0	0	4718	84601	
	10^4	1.15×10^{-8}	5.12×10^{-4}	0	0	4	33	
	10^5	4.35×10^{-8}	4.79×10^{-4}	0	0	4	33	
	10^6	1.14×10^{-6}	4.89×10^{-4}	0	0	4	33	
	10^7	3.99×10^{-6}	5.00×10^{-4}	0	0	4	33	
oscode	10^1	1.41×10^{-12}	4.88×10^{-1}	0	2716	2716	89408	
	10^2	1.44×10^{-11}	3.79×10^0	0	27270	27270	905938	
	10^3	5.58×10^{-11}	3.38×10^1	12	240737	240749	7965804	
	10^4	$\leq 5 \times 10^{-11}$	1.93×10^{-2}	137	0	137	4620	
	10^5	$\leq 3 \times 10^{-10}$	2.61×10^{-2}	198	0	198	6226	
	10^6	$\leq 5 \times 10^{-9}$	7.13×10^{-2}	504	0	504	17094	
	10^7	$\leq 4 \times 10^{-8}$	7.47×10^{-2}	465	0	465	18128	

Table 1: Accuracy, runtime and evaluation statistics of the algorithms considered when applied to (49). See Section 4.2 for a summary of the solvers being compared and their settings, and an explanation of column headers.

relative errors at $\varepsilon = 10^{-12}$ reported in Table 1 (solid lines), it also shows those at $\varepsilon = 10^{-6}$ (dashed lines). It further shows the same quantities for a 7,8th order Runge–Kutta method (denoted RK78) [31, 18] as a representative of many standard high-order methods, whose runtime is expected to grow as $\mathcal{O}(\lambda)$. The right-hand panel contains a gray shaded area whose upper edge serves as an upper bound on any data points (relative errors) that fall within it. This area is defined by the error reported for Kummer's phase function method in [11, Table 1], which being our reference for computing errors gives an upper bound. This is reflected in Table 1: for any measured errors lower than the reference we report only the upper bound.

Table 1 shows clearly the extremely quick convergence of the asymptotic method within ARDC at sufficiently large frequencies: at $\lambda \geq 10^2$, the number of function evaluations and steps become constant (≈ 2), causing the runtime to be constant as well. Towards $\lambda = 10^7$, only ≈ 2 Riccati iterations are required to achieve an estimated (local) relative error of 10^{-12} . At $\varepsilon = 10^{-12}$, ARDC achieves the same accuracy as the Kummer's phase function method, in the intermediate-to-large λ

regime, but is roughly 10 times faster. Fig. 5 illustrates this nicely, but also highlights that Kummer’s phase function method becomes significantly faster (comparable to ARDC) at $\varepsilon = 10^{-6}$, without the loss of accuracy, at all frequencies. In other words, the convergence curve (achieved versus requested accuracy) in the Kummer’s phase function implementation is closer to a step function than to a straight line.

`oscode` and the WKB marching method also achieve fast convergence at sufficiently large frequencies, but due to the fact that neither are adaptive in the order of the asymptotic expansion (*i.e.* the number of terms in the expansion) this happens later, at around $\lambda \geq 10^4$. This manifests itself as the low- λ “hill” in the left panel of Fig. 5 at $\varepsilon = 10^{-12}$, but disappears at the higher tolerance $\varepsilon = 10^{-6}$. Potentially due to the stepsize-update algorithm used by `oscode`, its number of steps, function evaluations, and therefore runtime, grows slowly rather than staying constant as the frequency increases. As with Kummer’s phase function method, at sufficiently high frequencies ($\lambda \geq 10^4$), setting a tolerance of $\varepsilon = 10^{-6}$ in `oscode` results in the same accuracy as setting $\varepsilon = 10^{-12}$ but at fewer function evaluations and steps, again due to the WKB expansion being highly accurate in this regime and to `oscode` potentially overestimating its local error.

Finally, the WKB marching method needs significantly fewer function evaluations (although achieves fewer digits of accuracy) at high frequencies because it asks the user to provide high-order derivatives of the frequency $\omega(t)$, therefore it need not use further evaluations of ω to compute said derivatives numerically.

Remark 10. *Three solvers (ARDC, the Kummer’s phase function method, and `oscode`) offer a dense output option, and do so by interpolating a slowly-varying phase function, therefore they all have evaluation times of $\mathcal{O}(10^{-6})$ s per new target.*

4.3 Special function evaluation: Legendre’s equation

Here we apply the proposed ARDC method to the rapid evaluation of Legendre functions of high degree ν . Such functions solve Legendre’s differential equation [47, Sec. 14.2]

$$(1 - t^2)u'' - 2tu' + \nu(\nu + 1)u = 0, \quad -1 < t < 1. \quad (51)$$

We test a range of integer ν values from 10 to 10^9 , and check accuracy against `scipy`’s evaluation of the Legendre polynomial $P_\nu(t)$. We solve on the solution interval $t \in [0.0, 0.9]$, with the internal steps of ARDC as test points.⁵ Initial conditions at $t_0 = 0$ are chosen to match the value and derivative of P_ν , expressible in terms of gamma functions [47, Chapter 14.5] (where the log gamma function is used to avoid roundoff at large ν).

Error and timing results are shown in Table 2, for tolerances of $\varepsilon = 10^{-12}$, $\varepsilon_h = 10^{-13}$, and the number of Chebyshev nodes in Riccati steps set to $n = 16$. They show a frequency-independent runtime, show that the required tolerance (up to that allowed by the condition number of the problem) is achieved.

Keeping in mind Remark 10, ARDC thus enables (at close to theoretical error bounds) the evaluation of $P_\nu(t)$ with a startup time of around 10^{-3} s, plus around 10^{-6} s per subsequent evaluation at each t argument, with both costs independent of ν for large ν . For comparison, `scipy`’s evaluation time grows with ν , taking around 1 s per evaluation at $\nu = 10^9$.

5 Conclusions

We presented an efficient numerical algorithm for solving linear second order ODEs of a single variable, posed as initial value problems (see (1)), whose solution may be highly oscillatory for some

⁵Since both $\omega(t) = \sqrt{\nu(\nu + 1)/(1 - t^2)}$ and $\gamma(t) = -t/(1 - t^2)$ have singularities at $t = \pm 1$, we defer analysis of this limit to future work. For now we merely state that empirically we are able to take $t_1 \rightarrow 1$ as ν grows.

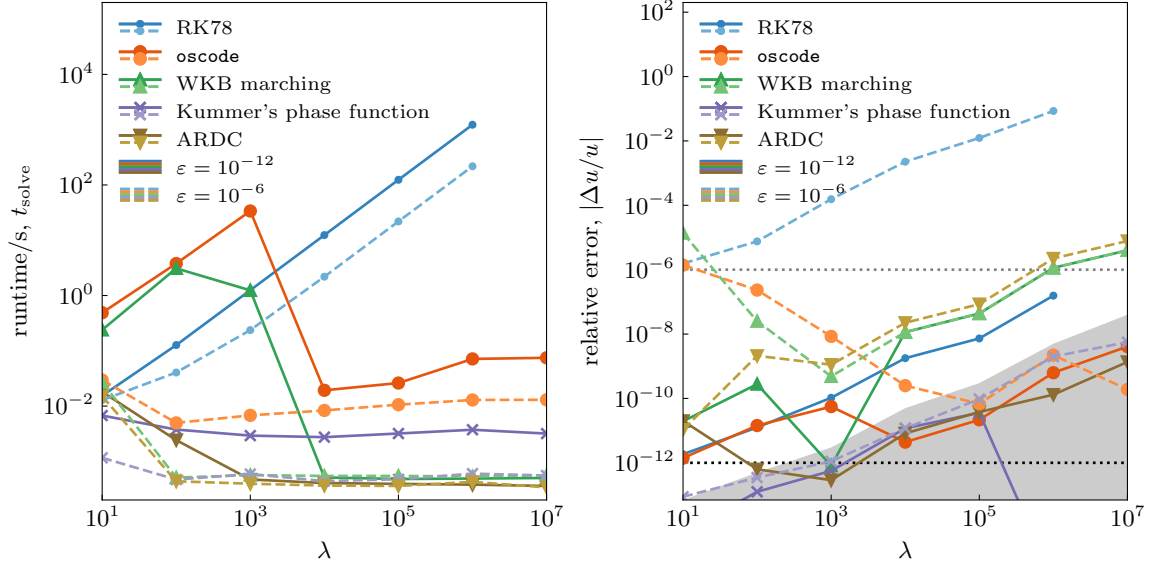


Figure 5: Performance comparison of the proposed ARDC method against other state-of-the-art methods for (49). The left panel shows the total runtime of the solvers listed in Section 4.2 as the frequency parameter λ is varied, for two different relative tolerance settings: runtimes with $\varepsilon = 10^{-12}$ are plotted with solid, and $\varepsilon = 10^{-6}$ with dashed lines. The right panel shows the corresponding relative error the solvers achieved at the end of the integration interval. The gray shaded region in this plot serves as an upper bound on any errors that fall within it, since the errors plotted here were computed using the Kummer’s phase function method as a reference, which is only accurate up to the upper edge of the gray region. This is consistent with the theoretical error minimum (45).

regions of the solution interval. It switches adaptively between a new defect correction iteration for the Riccati phase function (the logarithm of a solution in oscillatory regions), and a conventional Chebyshev collocation solver (in smooth regions). Both schemes are discretized to arbitrarily high order, and have step-size adaptivity. The resulting run time is independent of the maximum oscillation frequency. It improves over prior high-frequency solvers in several ways: it is efficient regardless of whether the solution oscillates or not; it is arbitrarily high-order accurate; it solves a more general problem by not imposing the restriction $\gamma = 0$ in (1); and it finds a nonoscillatory local phase function without needing a windowing method.

The proposed Riccati defect correction is asymptotic with respect to large ω , but we believe not in general convergent. However, we proved (Theorem 4) that, for analytic coefficients with $\omega(t)$ sufficiently large and ω' and γ sufficiently small in a ball, that (at the continuous level) it reduces the Riccati residual geometrically by a factor $\mathcal{O}(\omega)$ per iterate, temporarily up to a certain number of iterations which also scales as $\mathcal{O}(\omega)$. The constants are explicit in this theorem, and predict rapid residual reduction even when the ball over which ω is roughly constant is only a few oscillation periods across. We leave it to future work to analyze the discretized iteration (Section 2.2).

Numerical experiments in four ODEs demonstrate that the adaptivity achieves close to the requested tolerance, up to theoretical error bounds imposed by the condition number of the problem. They also show the solver’s high performance, allowing rapid solution times relative to existing oscillatory solvers at comparable accuracies.

We now discuss some future directions. Although we focused on initial value problems, much of the proposed scheme would carry over to the discretization of possibly-highly-oscillatory homo-

ν	$\max \Delta u/u $	t_{solve}/s	$n_{s,\text{osc}}$	$n_{s,\text{slo}}$	$n_{s,\text{tot}}$	n_f	n_{LS}
10^1	1.04×10^{-11}	6.28×10^{-3}	(0, 0)	(12, 12)	(12, 12)	3141	25
10^2	1.92×10^{-10}	3.21×10^{-2}	(35, 3)	(52, 52)	(87, 55)	14345	107
10^3	2.63×10^{-12}	1.75×10^{-3}	(10, 10)	(0, 0)	(10, 10)	1194	1
10^4	5.01×10^{-12}	1.44×10^{-3}	(10, 10)	(0, 0)	(10, 10)	1194	1
10^5	1.06×10^{-10}	1.36×10^{-3}	(10, 10)	(0, 0)	(10, 10)	1194	1
10^6	3.83×10^{-10}	1.31×10^{-3}	(10, 10)	(0, 0)	(10, 10)	1194	1
10^7	1.5×10^{-9}	1.27×10^{-3}	(10, 10)	(0, 0)	(10, 10)	1194	1
10^8	3.31×10^{-8}	1.23×10^{-3}	(10, 10)	(0, 0)	(10, 10)	1194	1
10^9	3.85×10^{-7}	1.24×10^{-3}	(10, 10)	(0, 0)	(10, 10)	1194	1

Table 2: Accuracy, runtime and evaluation statistics of the proposed ARDC method when applied to Legendre functions via their ODE (51). The degree is ν ; other column headers are identical to those in Table 1 and are explained in the text.

geneous two-point boundary value problems. Due to the linearity of the ODE, any set of auxiliary conditions can be satisfied as a post-processing step by solving the ODE with two sets of linearly independent initial conditions and linearly combining the resulting solutions. We note that a recent preprint addresses oscillatory ODEs with a slowly-varying inhomogeneous forcing term [51].

Within the scope of this work, we only allowed ω real. When ω is imaginary, any standard numerical solver will pick up the exponentially growing solution due to rounding error, which will quickly overpower the evanescent solution. However, in the case where physical decay conditions are known (such as quantum eigenvalue problems), it might be possible to use Riccati phase functions to impose these conditions in a stable fashion.

Spectral methods are usually applied over the entire solution interval (*e.g.* in [20]) rather than within a time-stepping framework. When applied locally and over a stepsize that can be changed adaptively, a degeneracy appears between the number of nodes n and the stepsize h , in that n can be increased and h can be decreased to lower the local error. Efficiency could be increased by determining the points at which the algorithm is supposed to switch between Riccati and Chebyshev steps *a priori*, or at least identifying large regions of the solution interval where the Chebyshev spectral method will need to be used, and solving the ODE in these regions with a quasi-linear spectral scheme with large n [53, 25].

On the analysis side, connecting residual error back to the solution error is a future goal; however, this appears quite technical in the oscillatory case [35].

Acknowledgments

We have benefited greatly from discussions with Jim Bremer, Charlie Epstein, Manas Rachh, and Leslie Greengard. The Flatiron Institute is a division of the Simons Foundation.

References

- [1] R. Adhikari, R. Dutt, A. Khare, and U. Sukhatme. “Higher-order WKB approximations in supersymmetric quantum mechanics”. In: *Physical Review A* 38.4 (1988), p. 1679.
- [2] F. J. Agocs, W. J. Handley, A. N. Lasenby, and M. P. Hobson. “Efficient method for solving highly oscillatory ordinary differential equations with applications to physical systems”. In: *Physical Review Research* 2.1 (2020), p. 013030.

- [3] F. J. Agocs, M. P. Hobson, W. J. Handley, and A. N. Lasenby. “Dense output for highly oscillatory numerical solutions”. In: *arXiv preprint arXiv:2007.05013* (2020).
- [4] F. J. Agocs. “(py)oscode: fast solutions of oscillatory ODEs”. In: *Journal of Open Source Software* 5.56 (2020), p. 2830. DOI: [10.21105/joss.02830](https://doi.org/10.21105/joss.02830). URL: <https://doi.org/10.21105/joss.02830>.
- [5] A. Arnold, N. B. Abdallah, and C. Negulescu. “WKB-based schemes for the oscillatory 1D Schrödinger equation in the semiclassical limit”. In: *SIAM journal on numerical analysis* 49.4 (2011), pp. 1436–1460.
- [6] R. Bellman. “Methods of nonlinear analysis”. In: Elsevier, 1970. Chap. 10.
- [7] C. M. Bender, S. Orszag, and S. A. Orszag. *Advanced mathematical methods for scientists and engineers I: Asymptotic methods and perturbation theory*. Vol. 1. Springer Science & Business Media, 1999.
- [8] M. V. Berry. “Asymptotics, superasymptotics, hyperasymptotics...” In: *Asymptotics beyond all orders*. Ed. by H. Segur, S. Tanveer, and H. Levine. Plenum, New York, 1991, pp. 1–14.
- [9] K. Böhmer and H. J. Stetter. *Defect correction methods*. Vol. 5. Springer, 1984.
- [10] J. P. Boyd. “The devil’s invention: asymptotic, superasymptotic and hyperasymptotic series”. In: *Acta Appl. Math.* 56.1 (1999).
- [11] J. Bremer. “On the numerical solution of second order ordinary differential equations in the high-frequency regime”. In: *Applied and Computational Harmonic Analysis* 44.2 (2018), pp. 312–349.
- [12] J. Bremer. “Phase function methods for second order linear ordinary differential equations with turning points”. In: *arXiv preprint arXiv:2209.14561* (2022).
- [13] J. Bremer and V. Rokhlin. “Improved estimates for nonoscillatory phase functions”. In: *Discrete and Continuous Dynamical Systems* 36.8 (2016), pp. 4101–4131. DOI: [10.3934/dcds.2016.36.4101](https://doi.org/10.3934/dcds.2016.36.4101).
- [14] P. Cea, P. Colangelo, G. Nardulli, G. Paiano, and G. Preparata. “WKB approach to the Schrödinger equation with relativistic kinematics”. In: *Physical Review D* 26.5 (1982), p. 1157.
- [15] E. D. Courant and H. S. Snyder. “Theory of the alternating-gradient synchrotron”. In: *Annals of physics* 3.1 (1958), pp. 1–48.
- [16] R. C. Davidson and Q. Hong. *Physics of intense charged particle beams in high energy accelerators*. World Scientific, 2001.
- [17] *NIST Digital Library of Mathematical Functions*. <http://dlmf.nist.gov/>, Release 1.1.7 of 2022-10-15. F. W. J. Olver, A. B. Olde Daalhuis, D. W. Lozier, B. I. Schneider, R. F. Boisvert, C. W. Clark, B. R. Miller, B. V. Saunders, H. S. Cohl, and M. A. McClain, eds. URL: <http://dlmf.nist.gov/9>.
- [18] *DOP853*. <http://www.unige.ch/hairet/software.html>. (Page with original Fortran code of DOP853.) URL: <http://www.unige.ch/~hairet/software.html>.
- [19] T. A. Driscoll, N. Hale, and L. N. Trefethen. *Chebfun Guide*. Pafnuty Publications, 2014. URL: <http://www.chebfun.org/docs/guide/>.
- [20] T. A. Driscoll, F. Bornemann, and L. N. Trefethen. “The chebop system for automatic solution of differential equations”. In: *BIT Numerical Mathematics* 48.4 (2008), pp. 701–723.
- [21] F. Einaudi and C. Hines. “WKB approximation in application to acoustic-gravity waves”. In: *Canadian Journal of Physics* 48.12 (1970), pp. 1458–1471.
- [22] B. Engquist, A. Fokas, E. Hairer, and A. Iserles. *Highly oscillatory problems*. Vol. 366. Cambridge University Press, 2009.

- [23] P. Filippi, A. Bergassoli, D. Habault, and J. P. Lefebvre. *Acoustics: basic physics, theory, and methods*. Elsevier, 1998.
- [24] G. Fiore. “The time-dependent harmonic oscillator revisited”. In: *arXiv preprint arXiv:2205.01781* (2022).
- [25] D. Fortunato, N. Hale, and A. Townsend. “The ultraspherical spectral element method”. In: *Journal of Computational Physics* 436 (2021), p. 110087.
- [26] W. M. Gentleman. “Implementing Clenshaw-Curtis quadrature, I methodology and experience”. In: *Communications of the ACM* 15.5 (1972), pp. 337–342.
- [27] W. M. Gentleman. “Implementing Clenshaw-Curtis quadrature, II computing the cosine transformation”. In: *Communications of the ACM* 15.5 (1972), pp. 343–346.
- [28] I. Gradshteyn and I. Ryzhik. *Table of Integrals, Series and Products*. 8th. New York: Academic, 2015.
- [29] A. Greenbaum and T. P. Chartier. *Numerical Methods*. Princeton University Press, 2012.
- [30] D. J. Griffiths and D. F. Schroeter. *Introduction to quantum mechanics*. Cambridge university press, 2018.
- [31] E. Hairer, G. Wanner, and S. P. Nørsett. *Solving Ordinary Differential Equations I*. Springer Berlin Heidelberg, 1993. DOI: [10.1007/978-3-540-78862-1](https://doi.org/10.1007/978-3-540-78862-1). URL: <https://doi.org/10.1007/978-3-540-78862-1>.
- [32] N. Hale and L. N. Trefethen. “Chebfun and numerical quadrature”. In: *Science China Mathematics* 55.9 (2012), pp. 1749–1760.
- [33] C. R. Harris et al. “Array programming with NumPy”. In: *Nature* 585.7825 (Sept. 2020), pp. 357–362. DOI: [10.1038/s41586-020-2649-2](https://doi.org/10.1038/s41586-020-2649-2). URL: <https://doi.org/10.1038/s41586-020-2649-2>.
- [34] R. D. Hazeltine and J. D. Meiss. *Plasma confinement*. Courier Corporation, 2003.
- [35] Z. Heitman, J. Bremer, and V. Rokhlin. “On the existence of nonoscillatory phase functions for second order ordinary differential equations in the high-frequency regime”. In: *Journal of Computational Physics* 290 (2015), pp. 1–27.
- [36] J. Helsing and R. Ojala. “On the evaluation of layer potentials close to their sources”. In: *J. Comput. Phys.* 227 (2008), pp. 2899–2921.
- [37] L. T. Hergt, F. J. Agocs, W. J. Handley, M. P. Hobson, and A. N. Lasenby. “Finite inflation in curved space”. In: *Physical Review D* 106.6 (Sept. 2022). DOI: [10.1103/physrevd.106.063529](https://doi.org/10.1103/physrevd.106.063529). URL: <https://doi.org/10.1103/physrevd.106.063529>.
- [38] J. Körner, A. Arnold, and K. Döpfner. “WKB-based scheme with adaptive step size control for the Schrödinger equation in the highly oscillatory regime”. In: *Journal of Computational and Applied Mathematics* 404 (2022), p. 113905.
- [39] R. Krivec. “Unified QLM for regular and arbitrary singular potentials”. In: *Applied Mathematics and Computation* 246 (2014), pp. 440–446.
- [40] R. Krivec and V. Mandelzweig. “Quasilinearization approach to computations with singular potentials”. In: *Computer Physics Communications* 179.12 (2008), pp. 865–867.
- [41] R. Krivec and V. Mandelzweig. “Quasilinearization method and WKB”. In: *Computer physics communications* 174.2 (2006), pp. 119–126.
- [42] H. R. Lewis Jr. “Motion of a time-dependent harmonic oscillator, and of a charged particle in a class of time-dependent, axially symmetric electromagnetic fields”. In: *Physical Review* 172.5 (1968), p. 1313.
- [43] K. K. Likharev. *Dynamics of Josephson junctions and circuits*. Routledge, 2022.

- [44] D. Logan. *Applied Mathematics*. 4th. Wiley, 2013.
- [45] V. Mandelzweig. “Quasilinear approach to summation of the WKB series”. In: *arXiv preprint quant-ph/0409137* (2004).
- [46] J. Martin and D. J. Schwarz. “WKB approximation for inflationary cosmological perturbations”. In: *Physical Review D* 67.8 (2003), p. 083512.
- [47] F. W. J. Olver, D. W. Lozier, R. F. Boisvert, and C. W. Clark, eds. *NIST Handbook of Mathematical Functions*. Cambridge University Press, 2010. URL: <http://dlmf.nist.gov>.
- [48] L. R. Petzold, L. O. Jay, and J. Yen. “Numerical solution of highly oscillatory ordinary differential equations”. In: *Acta numerica* 6 (1997), pp. 437–483.
- [49] G. Pritula, E. Petrenko, and O. Usatenko. “Adiabatic dynamics of one-dimensional classical Hamiltonian dissipative systems”. In: *Physics Letters A* 382.8 (2018), pp. 548–553. ISSN: 0375-9601. DOI: <https://doi.org/10.1016/j.physleta.2017.12.007>. URL: <https://www.sciencedirect.com/science/article/pii/S0375960117311714>.
- [50] G. Saxena and B. Ghosal. *Rubidium Atomic Clock: The Workhorse Of Satellite Navigation*. World Scientific Publishing Company, 2020. ISBN: 9789813279506. URL: <https://books.google.com/books?id=EGPcDwAAQBAJ>.
- [51] K. Serkh and J. Bremer. *Phase function methods for second order inhomogeneous linear ordinary differential equations*. 2022. arXiv: [2211.13744](https://arxiv.org/abs/2211.13744) [math.NA].
- [52] E. M. Stein and R. Shakarchi. *Complex analysis (Princeton Lectures in Analysis, No. 2)*. Princeton University Press, 2003.
- [53] L. N. Trefethen. *Spectral methods in MATLAB*. Vol. 10. Software, Environments, and Tools. Philadelphia, PA: Society for Industrial and Applied Mathematics (SIAM), 2000, pp. xviii+165.
- [54] P. Virtanen et al. “SciPy 1.0: Fundamental Algorithms for Scientific Computing in Python”. In: *Nature Methods* 17 (2020), pp. 261–272. DOI: [10.1038/s41592-019-0686-2](https://doi.org/10.1038/s41592-019-0686-2).
- [55] S. Winitzki. “Cosmological particle production and the precision of the WKB approximation”. In: *Physical Review D* 72.10 (2005), p. 104011.